Vilnius
University
Press

Turing instability and pattern formation of a fractional Hopfield reaction–diffusion neural network with transmission delay*

Jiazhe Lin[a] , **Jiapeng Li**[a] , **Rui Xu**[b,1]

[a]Computational Aerodynamic Research Institute,
China Aerodynamics Research and Development Center,
Mianyang 621000, China

[b]Complex Systems Research Center,
Shanxi University, Taiyuan 030006, China
xurui@sxu.edu.cn

Abstract. It is well known that integer-order neural networks with diffusion have rich spatial and temporal dynamical behaviors, including Turing pattern and Hopf bifurcation. Recently, some studies indicate that fractional calculus can depict the memory and hereditary attributes of neural networks more accurately. In this paper, we mainly investigate the Turing pattern in a delayed reaction–diffusion neural network with Caputo-type fractional derivative. In particular, we find that this fractional neural network can form steadily spatial patterns even if its first-derivative counterpart cannot develop any steady pattern, which implies that temporal fractional derivative contributes to pattern formation. Numerical simulations show that both fractional derivative and time delay have influence on the shape of Turing patterns.

Keywords: fractional derivative, neural network, Turing instability, pattern formation, reaction–diffusion.

1 Introduction

In the past few years, neural networks have attracted much attention in different fields of science and engineering, owing to their valuable applications in associative memory, combinatorial optimization, image processing and so on [5, 13]. Some of the above applications are based on the dynamical behavior analysis of neural networks [2]. Actually, neural networks are realized by large-scale integrated circuits, and the density of electromagnetic fields is generally not uniform. Therefore, in factual modeling, only considering the change of time seems to be not comprehensive when electrons are moving

---

[1]Corresponding author.

in asymmetric and nonuniform electromagnetic fields [21,22]. Due to the reaction–diffusion effect, neural networks have rich spatial and temporal dynamical behaviors, like various Turing patterns.

Spatial dynamics in reaction–diffusion systems was originally proposed by Turing in the work of [23], which mainly focuses on chemical reaction systems. This pioneer work not only established the theoretical foundation for understanding diverse patterns occurring in the natural world, but also opened a new research field, namely, pattern dynamics, which has received extensive attention and is still a hot topic in many fields such as species dynamics [7,27,28], medicine [26,31], networks [4,14,29]. Based on the reaction–diffusion theory of Turing, Chua and Goraş [4] investigated the phenomenon of pattern formation in cellular neural networks. Recently, Zhao et al. [29] studied the conditions of Hopf bifurcation and Turing instability in a reaction–diffusion neural network, where the corresponding model is described as follows:

$$
\begin{aligned}
\frac{\partial u(x,y,t)}{\partial t} &= d_1 \Delta u(x,y,t) - c_1 u(x,y,t) \\
&\quad + a_1 \tanh\bigl(v(x,y,t)\bigr) + b_1 \tanh\bigl(u(x,y,t)\bigr), \\
\frac{\partial v(x,y,t)}{\partial t} &= d_2 \Delta v(x,y,t) - c_2 v(x,y,t) \\
&\quad + a_2 \tanh\bigl(u(x,y,t)\bigr) + b_2 \tanh\bigl(v(x,y,t)\bigr)
\end{aligned}
\tag{1}
$$

in which $u(x,y,t)$, $v(x,y,t)$ stand for state variables of neurons at time t and spatial position (x,y); $c_i > 0$ ($i = 1,2$) denote the rates of resetting neuronic potential to the resting state in isolation; a_i, b_i ($i = 1,2$) represent connection weights; $\Delta = \partial^2/\partial x^2 + \partial^2/\partial y^2$ is the Laplacian operator in a two-dimensional space; $d_i > 0$ ($i = 1,2$) are diffusion coefficients of electrons among neurons.

Traditional neural networks, such as system (1), are mainly established from the view of integer-order derivatives, which can be described by classical ordinary differential equations. From the perspective of the application the integer-order derivative is used to describe some properties at a certain time in physical processes or some local properties of a certain position. In recent years, experimental research indicates that fraction-order derivatives provide an excellent tool for the description of memory and hereditary properties of various materials and processes [1,15]. Generally speaking, plenty of practical objects can be described clearly by the fractional differential equations due to their more degrees of freedom and infinite memory. Thus, the research of fractional neural networks has gained much attention, and some valuable results have been referred to [9–12,20].

Besides, due to the finite speed of signal transmission and amplifiers switching, time delay exists unavoidably in neural networks, which is known as transmission delay. Usually, the time delay is harmful to the stability performance of neural networks, causing oscillation, even chaos. Zhao et al. [30] introduced the transmission delay into a discrete-time Hopfield neural network model and showed that Hopf bifurcation occurs when the delay exceeds a critical value.

In [8], fractional calculus is used in electrical circuits that possess memory and hereditary properties, which is similar to the integrated circuits of Hopfield neural network.

Moreover, since fractional calculus is a generalization of conventional calculus, it is expected that fractional models will generally provide a more accurate description of the system dynamics than those based on classical differential equations [17]. In order to describe the memory and hereditary properties of Hopfield neural network, fractional order q is introduced into our model. Besides, time delay τ_1 and τ_2 are considered, which accounts for the finite speed of signal transmission and amplifiers switching in integrated circuits. Furthermore, it is generally assumed that the reaction–diffusion terms in system (1) play a conclusive role in pattern formation. A question arises naturally whether temporal fractional derivative has some relationship with pattern formation. To be specific, can the fractional reaction–diffusion neural network produce steadily spatial patterns even if its first-derivative counterpart cannot form any steady pattern? To this end, we consider the following delayed fractional reaction–diffusion neural network:

$$
\begin{aligned}
\frac{\partial^q u(x,y,t)}{\partial t^q} &= d_1 \Delta u(x,y,t) - c_1 u(x,y,t) \\
&\quad + a_1 f\big(v(x,y,t-\tau_1)\big) + b_1 f\big(u(x,y,t)\big), \\
\frac{\partial^q v(x,y,t)}{\partial t^q} &= d_2 \Delta v(x,y,t) - c_2 v(x,y,t) \\
&\quad + a_2 f\big(u(x,y,t-\tau_2)\big) + b_2 f\big(v(x,y,t)\big)
\end{aligned}
\tag{2}
$$

with initial condition

$$
u(x,y,\theta) = \phi_u(\theta), \quad v(x,y,\theta) = \phi_v(\theta), \quad (x,y) \in \Omega,
$$

satisfying

$$
\phi_u(\theta), \phi_v(\theta) \geqslant 0, \quad \theta \in [-\tau, 0), \quad \phi_u(0), \phi_v(0) > 0,
$$

and Neumann boundary condition

$$
\frac{\partial u(x,y,t)}{\partial n} = \frac{\partial v(x,y,t)}{\partial n} = 0, \quad (x,y) \in \partial\Omega,
$$

where $q \in (0,1]$ is the fractional order; τ_1 and τ_2 are transmission delay that reflects the time-lag effect; $f(\cdot)$ denotes the activation function, which maps the input to the output of the neuron; a square domain $\Omega = (0,L) \times (0,L)$ in which L is a positive bounded constant; n is the outward unit normal vector of the boundary $\partial\Omega$ that is assumed to be smooth; other variables and parameters are similar to those in system (1). For simplicity, let $\tau = \tau_1 = \tau_2$. The Neumann boundary condition implies that nothing enters this system and nothing exits from this system.

The main contributions of this paper can be summarized as follows: (i) By theoretical analysis and numerical simulations, the paper illustrates that temporal fractional derivative contributes to pattern formation in system (2); (ii) Fractional derivative can soften the stability conditions of the homogeneous steady state, which implies that when fractional-order $q = 1$, Hopf bifurcation occurs in system (2), but once $q < 1$, the homogeneous steady state may become stable; (iii) To avoid complicated and tedious MATLAB programming, numerical simulations are mainly completed by Simulink, which is more

efficient and can visually represent the interrelationships of neuron states; (IV) Numerical simulations indicate that the fractional derivative is related to the shape of the Turing pattern. Besides, as the fractional derivative decreases, it softens the Turing instability conditions of system (2).

This paper is organized as follows. In Section 2, we first analyze the existence of Hopf bifurcation and obtain the parameter sets, where the homogeneous steady state of system (2) is stable. Furthermore, we present and discuss the results of Turing instability and pattern formation, which will be illustrated by numerical simulations in Section 3. The paper ends with a conclusion in Section 4.

2 Hopf bifurcation and Turing instability

Throughout this paper, we address the following assumption holds.

(H1) $f \in C(\mathbb{R}, \mathbb{R})$, $f(0) = 0$, $zf(z) > 0$ for $z \in \mathbb{R}$, $z \neq 0$.

2.1 Hopf bifurcation

The homogeneous steady state of system (2) is $E_0 = (0, 0)$. In this subsection, we focus on the local asymptotic stability of E_0, which is useful for Turing instability analysis. The linear perturbation equations with respect to E_0 are

$$
\begin{aligned}
\frac{\partial^q u(x, y, t)}{\partial t^q} &= d_1 \Delta u(x, y, t) - c_1 u(x, y, t) \\
&\quad + \phi_1 v(x, y, t - \tau) + \varphi_1 u(x, y, t), \\
\frac{\partial^q v(x, y, t)}{\partial t^q} &= d_2 \Delta v(x, y, t) - c_2 v(x, y, t) \\
&\quad + \phi_2 u(x, y, t - \tau) + \varphi_2 v(x, y, t),
\end{aligned}
\tag{3}
$$

where $\phi_i = a_i f'(0)$, $\varphi_i = b_i f'(0)$, $i = 1, 2$. Expand the perturbation variables in the Fourier space

$$
\binom{u}{v} = \sum_{k_1=0}^{\infty} \sum_{k_2=0}^{\infty} \binom{r^1_{(k_1,k_2)}}{r^2_{(k_1,k_2)}} e^{\lambda t + i(k_1 x + k_2 y)},
\tag{4}
$$

where λ is the growth rate of perturbations in time t, i is the imaginary unit and $i^2 = -1$. In order to facilitate the analysis, let $k = k_1 = k_2$. Substituting (4) into (3), we obtain the characteristic equation as follows:

$$
\lambda^{2q} + p_1(k)\lambda^q + p_2(k) + re^{-2\tau\lambda} = 0,
\tag{5}
$$

where

$$
\begin{aligned}
p_1(k) &= k^2 d_1 + k^2 d_2 + c_1 + c_2 - \varphi_1 - \varphi_2, \\
p_2(k) &= (c_1 - \varphi_1 + k^2 d_1)(c_2 - \varphi_2 + k^2 d_2), \qquad r = -\phi_1 \phi_2.
\end{aligned}
$$

To find possible periodic solutions, which may bifurcate from a Hopf bifurcation point, let $\lambda = i\omega$ ($\omega > 0$ is a real number) be a root of (5). Separating the real and imaginary

parts yields

$$\cos(q\pi)\omega^{2q} + p_1(k)\cos\frac{q\pi}{2}\omega^q + p_2(k) + r\cos(2\omega\tau) = 0,$$
$$\sin(q\pi)\omega^{2q} + p_1(k)\sin\frac{q\pi}{2}\omega^q - r\sin(2\omega\tau) = 0. \tag{6}$$

It follows that

$$\omega^{4q} + 2p_1(k)\cos\frac{q\pi}{2}\omega^{3q} + \left[\left(p_1(k)\right)^2 + 2p_2(k)\cos(q\pi)\right]\omega^{2q}$$
$$+ 2p_1(k)p_2(k)\cos\frac{q\pi}{2}\omega^q + \left(p_2(k)\right)^2 - r^2 = 0. \tag{7}$$

From the first equation of (6) we have for $n = 0, 1, \ldots,$

$$\tau^{(n)} = \frac{1}{2\omega}\left\{\arccos\left[-\frac{1}{r}\left(\cos(q\pi)\omega^{2q} + p_1(k)\cos\frac{q\pi}{2}\omega^q + p_2(k)\right)\right] + 2n\pi\right\},$$

Define the bifurcation point of system (2) as $\tau_0 = \min\{\tau^{(n)}\}$. To establish the main results of this section, we list the following assumptions.

(H2) Equation (7) has no positive real root.
(H3) Equation (7) has at least one positive real root.
(H4) $(\Phi_1\Psi_1 + \Phi_2\Psi_2)/(\Psi_1^2 + \Psi_2^2) \neq 0$, where Φ_i, Ψ_i ($i = 1, 2$) will be defined in Lemma 2.

Define a parameter set

$$\Pi_1 = \left\{(c_1, c_2, \phi_1, \phi_2, \varphi_1, \varphi_2) \in \mathbb{R}_+^2 \times \mathbb{R}^4 \mid p_1(k) > 0, \ p_2(k) + r > 0\right\},$$

where E_0 is locally asymptotically stable when $\tau = 0$ and $q = 1$. For $\tau = 0$ and $q \in (0, 1)$, we first introduce the following lemma.

Lemma 1. (*See* [16].) *The following autonomous system*

$$\frac{\partial^q z}{\partial t^q} = Jz, \qquad z(0) = z_0,$$

where $0 < q < 1$, $z \in \mathbb{R}^n$, $J \in \mathbb{R}^{n \times n}$, is asymptotically stable if and only if $|\arg(\lambda_i)| > q\pi/2$ ($i = 1, 2, \ldots, n$). In this case, each component of the states decays towards 0 like t^{-q}. Also, this system is asymptotically stable if and only if $|\arg(\lambda_i)| \geqslant q\pi/2$ and those critical eigenvalues that satisfy $\|\arg(\lambda_i)\| = q\pi/2$ have geometric multiplicity one.

From Lemma 1 we obtain that the homogeneous steady state E_0 is locally asymptotically stable if the following inequalities hold: $|\arg(\lambda_i)| > q\pi/2$, $i = 1, 2$. Similarly, we define the following parameter set:

$$\Pi_2 = \left\{(c_1, c_2, \phi_1, \phi_2, \varphi_1, \varphi_2, q) \in \mathbb{R}_+^2 \times \mathbb{R}^4 \times (0, 1) \mid |\arg(\lambda_i)| > \frac{q\pi}{2}\right\},$$

where E_0 is locally asymptotically stable for $\tau = 0$ and $q \in (0, 1)$.

In conclusion, when $\tau = 0$, the homogeneous steady state E_0 is stable if the parameters φ_1 and φ_2 are in the set $\Pi_1 \cap \Pi_2$.

Lemma 2. *Let* $\lambda(\tau) = \mu(\tau) + \mathrm{i}\omega(\tau)$ *be the root of Eq.* (5) *near* $\tau = \tau_0$ *satisfying* $\mu(\tau_0) = 0$, $\omega(\tau_0) = \omega_0$, *then the following transversality condition holds*:

$$\mathrm{Re}\left[\frac{\mathrm{d}\lambda}{\mathrm{d}\tau}\right]\bigg|_{\tau=\tau_0} \neq 0.$$

Proof. Based on implicit function theorem, we calculate the derivative of Eq. (5) with respect to τ as follows: $\mathrm{d}\lambda/\mathrm{d}\tau = \Phi(\lambda)/\Psi(\lambda)$, where $\Phi(\lambda) = 2\lambda r e^{-2\tau\lambda}$, $\Psi(\lambda) = 2q\lambda^{2q-1} + p_1(k)q\lambda^{q-1} - 2\tau r e^{-2\tau\lambda}$. The real part of $\mathrm{d}\lambda/\mathrm{d}\tau$ at $\tau = \tau_0$ is $\mathrm{Re}[\mathrm{d}\lambda/\mathrm{d}\tau]|_{\tau=\tau_0} = (\Phi_1\Psi_1 + \Phi_2\Psi_2)/(\Psi_1^2 + \Psi_2^2)$, where Φ_1 and Φ_2 are the real and imaginary parts of $\Phi(\mathrm{i}\omega_0)$, respectively; Ψ_1 and Ψ_2 are the real and imaginary parts of $\Psi(\mathrm{i}\omega_0)$, respectively. Based on assumption (H4), the transversality condition is met.   □

Theorem 1. *For system* (2)*, the following results hold*:

  (i) *If* (φ_1, φ_2) *stays in the set* $\Pi_1 \cap \Pi_2$ *and* (H2) *holds, then the homogeneous steady state is locally asymptotically stable for* $\tau \in [0, +\infty)$.

 (ii) *If* (φ_1, φ_2) *stays in the set* $\Pi_1 \cap \Pi_2$ *and* (H3), (H4) *hold, then*

   (a) *The homogeneous steady state is locally asymptotically stable for* $\tau \in [0, \tau_0)$.

   (b) *System* (2) *undergoes a Hopf bifurcation at the homogeneous steady state when* $\tau = \tau_0$, *i.e., it has a branch of periodic solutions bifurcating from the homogeneous steady state near* $\tau = \tau_0$.

Choose (φ_1, φ_2) as free parameters and project the parameter sets Π_1 and Π_2 into a two-dimensional space with respect to (φ_1, φ_2). From the conditions of parameter sets Π_1 and Π_2 we draw the stability regions of E_0. In Fig. 1, the parameter set Π_1 corresponds to region A (green), while Π_2 corresponds to the region B (yellow). Region B implies that temporal fractional derivative can enlarge the stability region of E_0.
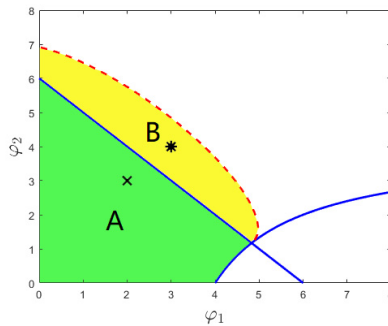

Figure 1. The bifurcation diagram of the parameters φ_1 and φ_2 with $c_1 = 2$, $c_2 = 4$, $\phi_1 = -4$, $\phi_2 = 2$, $\tau = 0$, where the position of the mark "$\times$" is $(2, 3)$, and the one of "$*$" is $(3, 4)$. The two solid (blue) lines come from the conditions of Π_1, while the dashed (orange) line comes from the condition of Π_2.

2.2 Turing instability

Next, we will verify that system (2) can form steadily spatial patterns even if its first-derivative counterpart cannot develop any steady pattern. Firstly, we discuss the Turing instability of system (2). The unbalanced changes of phases, corresponding to Turing branches, are the transitions of system (2) from the uniform state to the oscillatory state [29, 32]. After the process, the formed patterns are called Turing patterns. From (5) we obtain the necessary conditions for causing Turing instability when $\tau = 0$:

$$\varphi_1 + \varphi_2 - c_1 - c_2 < 0, \tag{8}$$

$$(c_1 - \varphi_1)(c_2 - \varphi_2) - \phi_1\phi_2 > 0, \tag{9}$$

$$d_1 d_2 k^4 - \big[(\varphi_2 - c_2)d_1 + (\varphi_1 - c_1)d_2\big]k^2$$
$$+ (c_1 - \varphi_1)(c_2 - \varphi_2) - \phi_1\phi_2 < 0. \tag{10}$$

Conditions (8)–(10) indicate that system (2) is unstable for some perturbations to the wave number k. Thus, we obtain that $\det_k(J) = 0$ at the critical value. That is to say, Turing bifurcation occurs when $\mathrm{Im}(\lambda_k) = 0$, $\mathrm{Re}(\lambda_k) = 0$ at $k = k_c \neq 0$ [19]. When Turing patterns come into being, the wave number k_c satisfies

$$k_c^2 = \frac{(\varphi_2 - c_2)d_1 + (\varphi_1 - c_1)d_2}{2d_1 d_2}.$$

Based on above discussions, we get the following result.

Lemma 3. *If the parameters φ_1 and φ_2 are in the set $\Pi_1 \cap \Pi_2$ and the following conditions hold*

$$d_1(\varphi_2 - c_2) + d_2(\varphi_1 - c_1) > 0, \tag{11}$$

$$\big[d_1(\varphi_2 - c_2) + d_2(\varphi_1 - c_1)\big]^2 - 4d_1 d_2\big[(c_1 - \varphi_1)(c_2 - \varphi_2) - \phi_1\phi_2\big] > 0, \tag{12}$$

then Turing instability in system (2) occurs when $\tau = 0$.

When $\tau \neq 0$, Turing instability occurs when $\lambda \to 0$, namely, $p_2(k) + r \to 0$, and then we have the following Turing instability curve:

$$\varphi_2^*(\varphi_1) = c_2 + k^2 d_2 - \frac{\phi_1\phi_2}{c_1 - \varphi_1 + k^2 d_1}.$$

Letting $\varphi_2(k) = \varphi_2(k+1)$ yields

$$\varphi_1^*(k,\, k+1) = \frac{2c_1 + (2k^2 + 2k + 1)d_1}{2} \pm \sqrt{\frac{(2k+1)^2 d_1^2}{4} - \frac{\phi_1\phi_2 d_1}{d_2}}.$$

Denote

$$\Pi_3 = \big\{(c_1, c_2, \phi_1, \phi_2, \varphi_1, \varphi_2) \in \mathbb{R}_+^2 \times \mathbb{R}^4 \,\big|\, (11) \text{ and } (12) \text{ hold}\big\}.$$

We set (φ_1, φ_2) as free parameters, then project the parameter set Π_3 into a two-dimensional space with respect to (φ_1, φ_2). From Fig. 2 we observe that $\Pi_1 \cap \Pi_2 \cap \Pi_3$ corresponds with regions C (green) and D (yellow), where the Turing instability occurs.
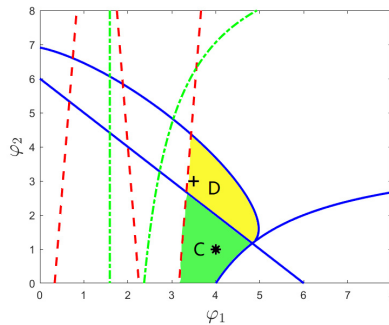
Figure 2. The bifurcation diagram of the parameters φ_1 and φ_2 with $d_1 = 0.1$, $d_2 = 1.6$, $c_1 = 2$, $c_2 = 4$, $\phi_1 = -4$, $\phi_2 = 2$, where the position of the mark "$*$" is $(4, 1)$ and the one of "$+$" is $(3.5, 3)$. The dashed (red) lines come from the conditions of Π_3, while the dot-and-dash (green) lines corresponds to $\varphi_2^*(\varphi_1)$ when $k = 2$.

When the fraction order $q = 1$, the Turing instability region only consists of region C. That is to say, region D is the enlarged region, where Turing instability is caused by fractional derivatives and reaction–diffusion terms together.

Theorem 2. *If (φ_1, φ_2) stays in $\Pi_1 \cap \Pi_2 \cap \Pi_3$, we obtain the following results:*

(i) *For $\varphi_1 \in [\varphi_1^*(k-1, k), \varphi_1^*(k, k+1))$, system (2) will undergoes k-mode Turing bifurcation at $\varphi_2 = \varphi_2^*(\varphi_1)$;*

(ii) *When $\varphi_1 = \varphi_1^*(k, k+1)$, $(k, k+1)$-mode Turing–Turing bifurcation occurs at $\varphi_2 = \varphi_2^*(\varphi_1^*(k, k+1))$.*

Remark 1. Usually, the curves of $\varphi_2^*(\varphi_1)$ with $k \in \mathbb{N}$ may reduce the area of Turing instability region. In Fig. 2, regions C and D are exactly below the curve of $\varphi_2^*(\varphi_1)$ with $k = 2$, and the Turing–Turing bifurcation point with $k = 1$ is on the left side of regions C and D. Thus, in this paper, the curves of $\varphi_2^*(\varphi_1)$ with $k \in \mathbb{N}$ make no difference with the Turing instability region.

3   Numerical simulations

Numerical algorithms for reaction–diffusion systems are often complicated, which need tedious MATLAB programming. Garvie [6] proposed a semiimplicit (in time) finite-difference scheme to approximate the solutions of reaction–diffusion systems. The semi-implicit method means this algorithm involves approximations at the current time level t_n and at the previous time level t_{n-1}. The corresponding algorithm is reduced to a sparse, banded and linear system of algebraic equations. In this section, we use Simulink to simplify the programming, which is more efficient and visually represents the interrelationships of neuron states. Simulink is graphical programming that is easy for nonprofessional scholars to program and realize the equivalent effect gained by MATLAB code. Besides, we can utilize user-defined MATLAB function blocks in Simulink, which takes full advantage of MATLAB code and Simulink.

Firstly, we give the following result about the Laplacian operator, which is used for the approximate calculation of reaction–diffusion terms. By means of the finite-difference scheme mentioned in [6, 25], the Laplacian with respect to the concentration field w in the node (i, j) is calculated along the x and y directions simultaneously:

$$\Delta^2 w(i, j, t_n) \approx \frac{\Delta_x^2 w(i, j, t_n)}{h_x^2} + \frac{\Delta_y^2 w(i, j, t_n)}{h_y^2}, \tag{13}$$

where

$$\Delta_x^2 w(i, j, t_n) = w(i + 1, j, t_n) - 2w(i, j, t_n) + w(i - 1, j, t_n),$$
$$\Delta_y^2 w(i, j, t_n) = w(i, j + 1, t_n) - 2w(i, j, t_n) + w(i, j - 1, t_n).$$

h_x and h_y in Eq. (13) are x and y grid spacings, respectively. Assume $h = h_x = h_y$ and discretize Laplacian operation in a two-dimensional domain Ω:

$$\Delta^2 w(i, j, t_n) \approx \frac{w(i + 1, j, t_n) + w(i - 1, j, t_n)}{h^2} - \frac{4w(i, j, t_n)}{h^2}$$
$$+ \frac{w(i, j + 1, t_n) + w(i, j - 1, t_n)}{h^2}. \tag{14}$$

From (14) the two-dimensional Laplacian operator is

$$\Delta^2 \approx L = \frac{1}{h^2} \begin{bmatrix} 0 & 1 & 0 \\ 1 & -4 & 1 \\ 0 & 1 & 0 \end{bmatrix}.$$

Following the approach of the modified Adams–Bashforth–Moulton predictor–corrector scheme mentioned in [3], we derive the approximate numerical values of the fractional derivatives with delay. Denote Δt as the time-step. Consider a uniform grid $\{t_n = n\Delta t: n = -k, -k + 1, \ldots, -1, 0, 1, \ldots, N\}$, where k and N are integers such that $k = \tau/\Delta t$ and $N = T/\Delta t$. Discretize the initial condition

$$u(t_j) = \phi_u(t_j), \quad v(t_j) = \phi_v(t_j), \quad j = -k, -k + 1, \ldots, -1, 0.$$

Besides, the delayed terms can be rewritten as follows:

$$u(t_j - \tau) = u(j\Delta t - k\Delta t) = u(t_{j-k}),$$
$$v(t_j - \tau) = v(j\Delta t - k\Delta t) = v(t_{j-k}),$$

where $j = 0, 1, \ldots, N$. The iteration formulas from $u(t_n), v(t_n)$ to $u(t_{n+1}), v(t_{n+1})$ are

$$u(t_{n+1}) = \phi_u(0) + \frac{(\Delta t)^q}{\Gamma(q + 2)} F_1\big(t_{n+1}, \tilde{u}(t_{n+1}), \tilde{v}(t_{n+1})\big)$$
$$+ \frac{h^q}{\Gamma(q + 2)} \sum_{j=0}^{n} a_{j,n+1} F_1\big(t_j, u(t_j), v(t_j)\big),$$

$$v(t_{n+1}) = \phi_v(0) + \frac{(\Delta t)^q}{\Gamma(q+2)} F_2\big(t_{n+1}, \tilde{u}(t_{n+1}), \tilde{v}(t_{n+1})\big)$$

$$+ \frac{h^q}{\Gamma(q+2)} \sum_{j=0}^{n} a_{j,n+1} F_2\big(t_j, u(t_j), v(t_j)\big),$$

where the discrete right-hand terms in system (2) are

$$F_1\big(t_n, u(t_n), v(t_n)\big) = d_1 \Delta u(t_n) - c_1 u(t_n) + a_1 f(v_{n-k}) + b_1 f\big(u(t_n)\big),$$
$$F_2\big(t_n, u(t_n), v(t_n)\big) = d_2 \Delta v(t_n) - c_2 v(t_n) + a_2 f(u_{n-k}) + b_2 f\big(v(t_n)\big),$$

and the predictor terms are

$$\tilde{u}(t_{n+1}) = \phi_u(0) + \frac{1}{\Gamma(q)} \sum_{j=0}^{n} b_{j,n+1} F_1\big(t_j, u(t_j), v(t_j)\big),$$

$$\tilde{v}(t_{n+1}) = \phi_v(0) + \frac{1}{\Gamma(q)} \sum_{j=0}^{n} b_{j,n+1} F_2\big(t_j, u(t_j), v(t_j)\big).$$

In addition, $a_{j,n+1}$ and $b_{j,n+1}$ are defined as

$$a_{j,n+1} = \begin{cases} n^{q+1} - (n-q)(n+1)^q & \text{if } j = 0, \\ (n-j+2)^{q+1} + (n-j)^{q+1} - 2(n-j+1)^{q+1} & \text{if } 1 \leqslant j \leqslant n, \\ 1 & \text{if } j = n+1, \end{cases}$$

$$b_{j,n+1} = \frac{(\Delta t)^q}{q}\big((n+1-j)^q - (n-j)^q\big).$$

System (2) is simulated numerically in a 100×100 two-dimensional square region. Time step and space step are set as 0.005 and 0.5, respectively, which needs large amount of computation but ensures the accuracy of numerical simulations. Diffusion coefficients (d_1, d_2) are chosen as $(0.1, 1.6)$. Besides, $c_1 = 2$, $c_2 = 4$, $a_1 = -4$, $a_2 = 2$. b_1 and b_2 are chosen as free parameters. Simulink construction of system (2), as we can see in Fig. 3, consists of some blocks and lines. Each block can realize different functions and is connected with others by data flow lines. The main blocks are 2D Convolution and user-defined MATLAB function. The 2D convolution completes the approximate calculation of the reaction–diffusion terms by two-dimensional Laplacian operator L. The user-defined MATLAB function realizes the integration of the right-hand terms in system (2) by the above modified Adams–Bashforth–Moulton predictor–corrector scheme.

When fractional order $q = 1$ and $\tau = 0$, system (2) becomes a first-derivative system. Activation function $f(\cdot)$ is selected as $\tanh(\cdot)$, where $b_1 = \varphi_1$ and $b_2 = \varphi_2$. Set (b_1, b_2) as $(4, 1)$ (marked by "$*$") and $(3.5, 3)$ (marked by "+"), respectively (as we can see in Fig. 2). Figures 4 and 5 are the two-dimension spatial states of neurons $u(x, y, t)$ and $v(x, y, t)$ at some moments, respectively. On account of diffusion, neuronic states not only vary in time, but also change in space. What is interesting is that spatial states take
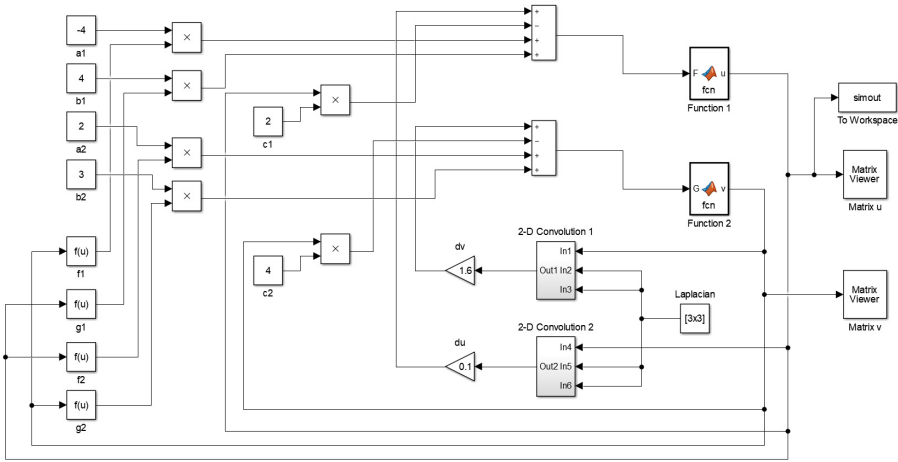
Figure 3. Simulink construction of system (2) with $q \in (0, 1)$.

on particular shapes. Comparing the figures of $u(x, y, t)$, $v(x, y, t)$($T = 50$) with the figures of $u(x, y, t)$, $v(x, y, t)$ ($T = 100$) in Fig. 4, we observe that system (2) forms steady Turing patterns. Furthermore, when (b_1, b_2) is $(3.5, 3)$, we observe in Fig. 5 that as the time T increases from 50 to 100, the figures of $u(x, y, t)$, $v(x, y, t)$ ($T = 50$) are different from the figures of $u(x, y, t)$, $v(x, y, t)$ ($T = 100$), which means that under this condition, system (2) cannot induce any steady Turing pattern.

As we can observe in Fig. 6, system (2) with $q = 0.79$ can form steady spatial patterns. Comparing it with Fig. 5, we know that system (2) form steadily spatial patterns even if its first-derivative counterpart cannot develop any steady pattern. Hence, these patterns are induced by temporal fractional derivative and reaction–diffusion terms together, which corresponds with region D in Fig. 2. Furthermore, to investigate the relationship between fractional derivative and Turing pattern, we change the fractional order q as 0.72 or 0.87. From Figs. 7 and 8 we observe that the shape of Turing patterns varies with the fractional order q. Obviously, when $q = 0.72$, the patterns of $u(x, y, t)$ and $v(x, y, t)$ become various steady types. When $q = 0.87$, the stability performance of the patterns of $u(x, y, t)$ and $v(x, y, t)$ is a little weak. In Fig. 8, when the time T increases from 50 to 100, the center patterns change to some extent.

It rises a question that whether temporal fractional derivative has some relationship with the locally asymptotical stability region or Turing instability region with respect to (φ_1, φ_2). From the left figure in Fig. 9 we obtain that the stability region of E_0 varies with fractional order q. As q increases from 0.72 to 0.79, the stability region of E_0 loses region D instead. Increasing q from 0.79 to 0.87 continuously, the stability region does not contain region C, namely, when $q = 0.87$, E_0 is stable when (φ_1, φ_2) only stays in regions A and B. Besides, we wonder how the Turing instability region induced by fractional derivatives and reaction–diffusion terms together varies with fractional order q. From the right figure in Fig. 9, when $q = 0.72$, the Turing instability region induced by fractional derivatives and reaction–diffusion terms together consists of regions E, F and G.
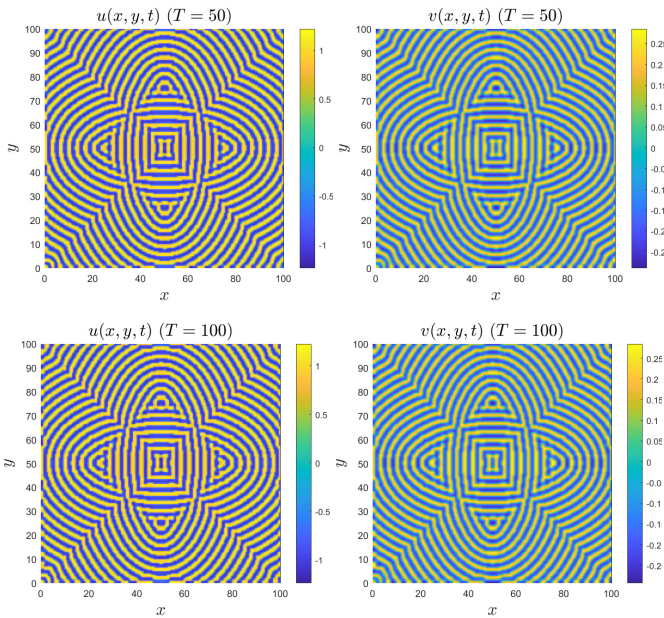
Figure 4. The steadily spatial patterns of $u(x, y, t)$ and $v(x, y, t)$ of system (2) in two-dimension square domain with $\tau = 0$, $q = 1$, $d_1 = 0.1$, $d_2 = 1.6$, $c_1 = 2$, $c_2 = 4$, $a_1 = -4$, $a_2 = 2$, $b_1 = 4$ and $b_2 = 1$. The initial condition is chosen as $u(0) = ((x-50)^2 + 0.2(y-50)^2) < 250$, $v(0) = (0.2(x-50)^2 + (y-50)^2) < 250$.
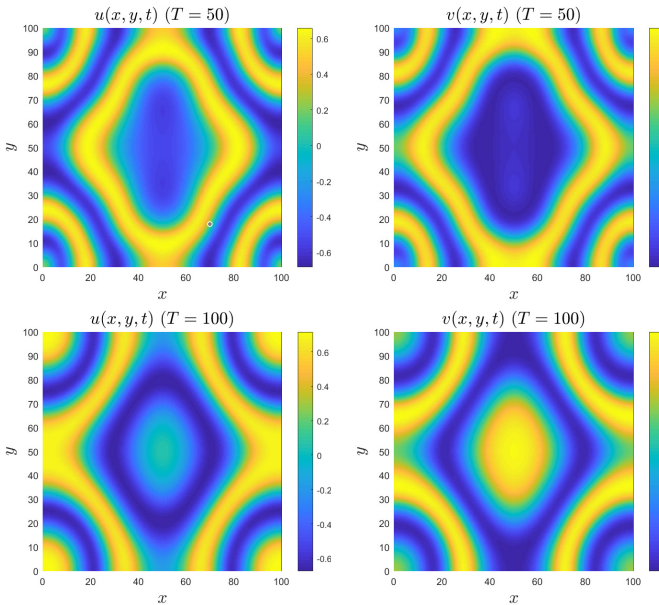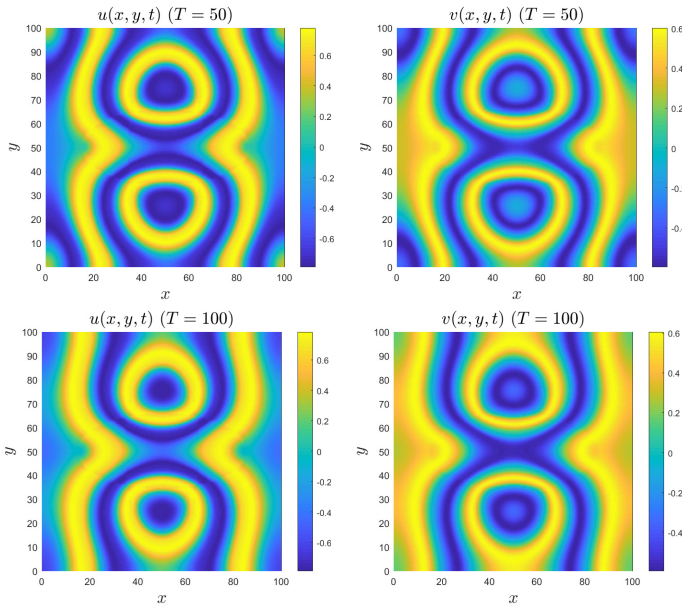

Figure 5. The unsteadily spatial patterns of $u(x, y, t)$ and $v(x, y, t)$ of system (2) in two-dimension square domain with $q = 1$, $b_1 = 3.5$ and $b_2 = 3$ and other parameters are similar to those in Fig. 4.

Figure 6. The steadily spatial patterns of $u(x, y, t)$ and $v(x, y, t)$ for system (2) in two-dimension square domain with $q = 0.79$, $b_1 = 3.5$ and $b_2 = 3$ and other parameters are similar to those in Fig. 5.
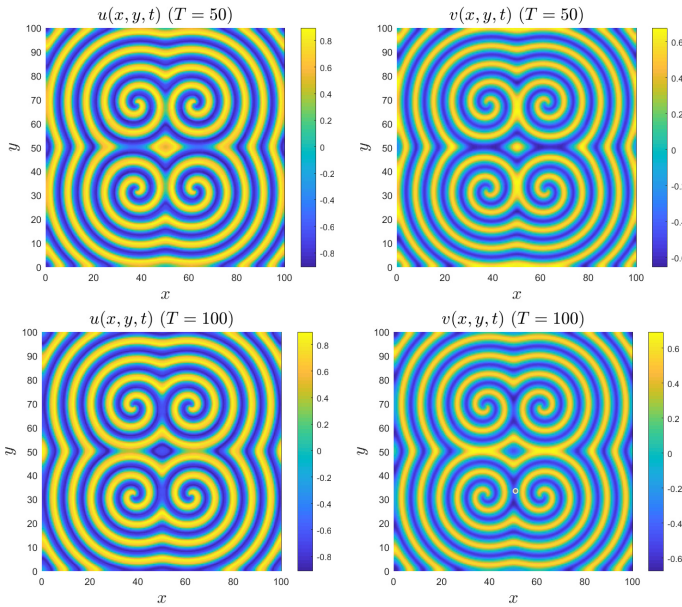

Figure 7. The steadily spatial patterns of $u(x, y, t)$ and $v(x, y, t)$ for system (2) in two-dimension square domain with $q = 0.72$ and other parameters are similar to those in Fig. 6.
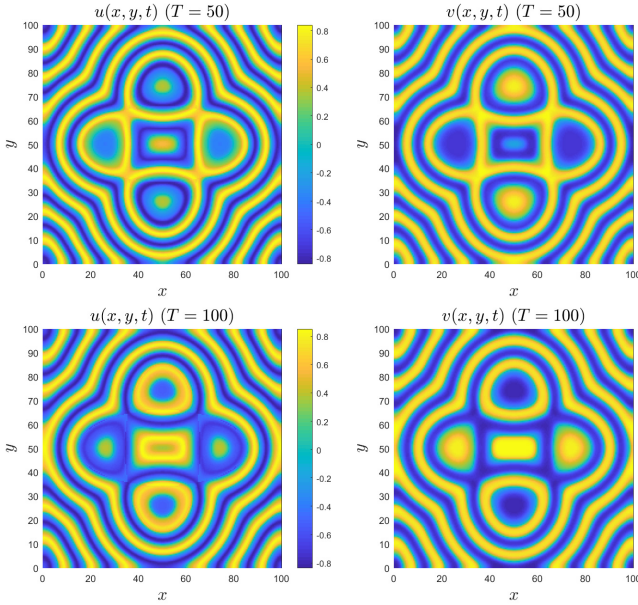
Figure 8. The unsteadily spatial patterns of $u(x, y, t)$ and $v(x, y, t)$ for system (2) in two-dimension square domain with $q = 0.87$ and other parameters are similar to those in Fig. 6.
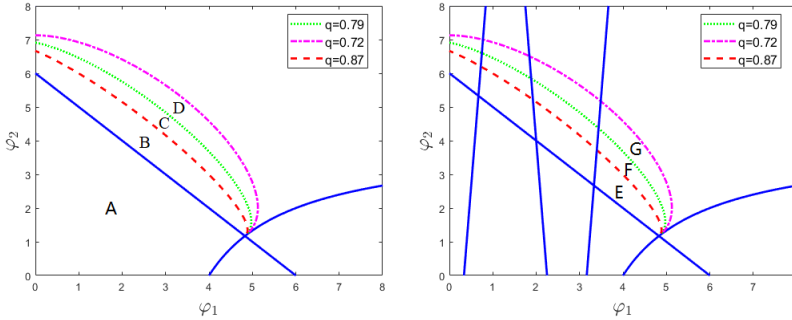

Figure 9. The bifurcation diagram of the parameters φ_1 and φ_2 with different fractional orders.

As q increases, the corresponding Turing instability region shrinks to region E, that is to say, when (φ_1, φ_2) stays in regions F and G, system (2) with $q = 0.87$ cannot form steady Turing patterns.

Remark 2. Due to that time delay widely exists in the neural network, we investigate the impact of transmission delay on Turing patterns. As we observe in Fig. 10, the patterns of $u(x, y, t)$ and $v(x, y, t)$ are more complicated than the patterns of those in Figs. 4–5 (a nondelay integer-order subsystem of system (2)) and Figs. 6–8 (a nondelay fractional-order subsystem of system (2)). Compared with Fig. 6, as τ increase from 0 to 0.6, Turing patterns change unpredictably and become unstable.
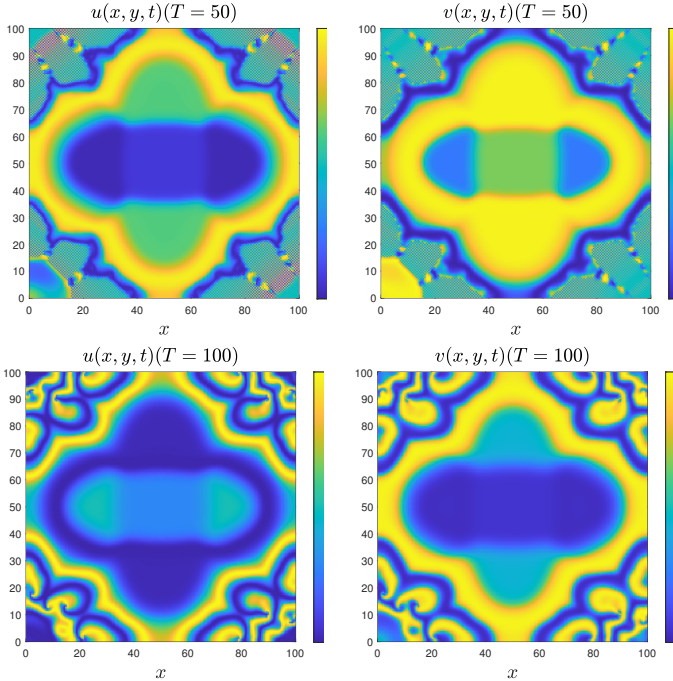
Figure 10. The unsteadily spatial patterns of $u(x, y, t)$ and $v(x, y, t)$ for system (2) in two-dimension square domain with $q = 0.79$, $\tau = 0.6$ and other parameters are similar to those in Fig. 6.
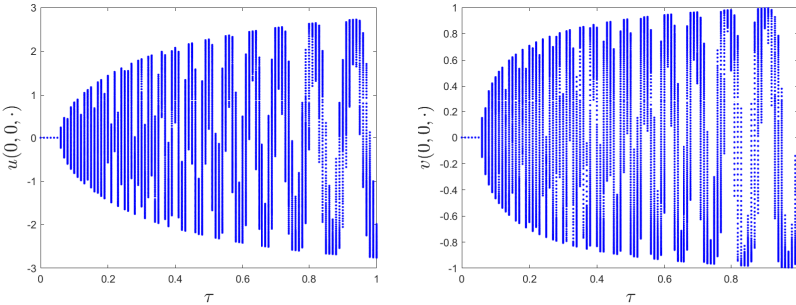

Figure 11. The bifurcation diagrams of $u(0, 0, \cdot)$ and $v(0, 0, \cdot)$ with respect to the parameter $\tau \in [0, 1]$.

Remark 3. As shown in Fig. 11, the central points of $u(x, y, t)$ and $v(x, y, t)$ are selected to study the bifurcation diagrams of system (2) with respect to transmission delay τ. $u(0, 0, \cdot)$ and $v(0, 0, \cdot)$ stay in stable state when $\tau < \tau_0 = 0.06$ and oscillate greatly as τ exceeds τ_0, where τ_0 can be seen as the critical value of Hopf bifurcation. Hence, as the transmission delay increases, Turing patterns lose its stability, and state variables of neurons vary in both time and space. Furthermore, when $\tau < \tau_0$ and fractional order is in a certain section, a stable Turing pattern may occur, which is induced by temporal

fractional derivative and reaction–diffusion terms together; when $\tau > \tau_0$, no matter how fractional order changes, the stable Turing pattern is hard to form.

4 Conclusion

In this paper, we proposed a delayed reaction–diffusion neural network with the Caputo-type fractional derivative. The condition of Hopf bifurcation was obtained firstly through analyzing relevant characteristic equation, while the condition of Turing instability was derived following the pattern dynamics theory proposed by [23]. Especially, we found that fractional derivative has a certain relationship with Hopf bifurcation and Turing pattern. To be specific, the fractional derivative could enlarge the stability region of homogeneous steady state E_0 concerning (φ_1, φ_2), which means that when the first-derivative counterpart of system (2) is unstable at E_0, but once introducing fractional derivative, E_0 may become stable again. Besides, as the fraction derivative decreases, it softens the Turing instability conditions of system (2). With the help of Simulink, we obtained the approximation solutions of system (2). Numerical simulations show that temporal fractional derivative contributes to Turing patterns in system (2), which accords with the previous theoretical analysis. Meanwhile, we found that the shape of the Turing pattern is related to the fraction order and the time delay.

Pattern dynamics in neural networks with diffusion has been investigated in [4,14,29], but previous research does not consider fractional derivative. In our study, we illustrate the impact of fractional derivative on spatial and temporal dynamics for system (2) and obtain plenty of meaningful findings. [29] obtained the amplitude equations for system (1) and studied the selection of Turing patterns. Due to the existence of fractional derivative, it is difficult for us to obtain the amplitude equations of system (2). In our further research, we will try to improve some classic methods, such as multiple-scale analysis, to obtain the amplitude equations for fractional reaction–diffusion systems.

The spatial dynamics analysis of reaction–diffusion neural networks not only reveals some properties of integrated circuits that are used to build neural networks, where a Turing pattern corresponds to a steady state that leads to nonuniformly spatial oscillation, but also illustrates many biological phenomena such as normal neuron firing in the brain [18] or biological disorders such as fibrillation [24].

References

1. T.J. Anastasio, The fractional-order dynamics of brainstem vestibule-oculomotor neurons, *Biol. Cybern.*, **72**:69–79, 1994, https://doi.org/10.1007/BF00206239.

2. G. Bao, Z. Zeng, Analysis and design of associative memories based on recurrent neural network with discontinuous activation functions, *Neurocomputing*, **77**(1):101–107, 2012, https://doi.org/10.1016/j.neucom.2011.08.026.

3. S. Bhalekar, V. Daftardar-Gejji, A predictor-corrector scheme for solving nonlinear delay differential equations of fractional order, *Fract. Calc. Appl. Anal.*, **1**:1–9, 2011.

4. L.O. Chua, L. Goraş, Turing patterns in cellular neural networks, *Int. J. Electron.*, **79**(6):719–736, 1995, https://doi.org/10.1080/00207219508926307.

5. L.O. Chua, L. Yang, Cellular neural networks: Applications, *IEEE Trans. Circuits Syst.*, **35**(10):1273–1290, 1988, https://doi.org/10.1109/31.7601.

6. M. Garvie, Finite difference schemes for reaction–diffusion equations modeling predator–prey interactions in MATLAB, *Bull. Math. Biol.*, **69**:931–956, 2007, https://doi.org/10.1007/s11538-006-9062-3.

7. B. Han, Z. Wang, Turing patterns of a Lotka–Volterra competitive system with nonlocal delay, *Int. J. Bifurcation Chaos Appl. Sci. Eng.*, **28**(7):1830021, 2018, https://doi.org/10.1142/S0218127418300215.

8. T. Hartley, C. Lorenzo, H. Qammer, Chaos in a fractional order Chua's system, *IEEE Trans. Circuits Syst. I: Fundamental Theory and Applications*, **42**(8):485–490, 1995, https://doi.org/10.1109/81.404062.

9. C. Huang, J. Cao, Impact of leakage delay on bifurcation in high-order fractional BAM neural networks, *Neural Netw.*, **98**:223–235, 2018, https://doi.org/10.1016/j.neunet.2017.11.020.

10. C. Huang, J. Cao, M. Xiao, A. Alsaedi, T. Hayat, Bifurcations in a delayed fractional complex-valued neural network, *Appl. Math. Comput.*, **292**(1):210–227, 2017, https://doi.org/10.1016/j.amc.2016.07.029.

11. C. Huang, J. Cao, M. Xiao, A. Alsaedi, T. Hayat, Effects of time delays on stability and Hopf bifurcation in a fractional ring-structured network with arbitrary neurons, *Commun. Nonlinear Sci. Numer. Simul.*, **57**:1–13, 2018, https://doi.org/10.1016/j.cnsns.2017.09.005.

12. C. Huang, Y. Meng, J. Cao, New bifurcation results for fractional BAM neural network with leakage delay, *Chaos Solitons Fractals*, **100**:31–44, 2017, https://doi.org/10.1016/j.chaos.2017.04.037.

13. B. Kosko, Adaptive bidirectional associative memories, *Appl. Opt.*, **26**(23):4947–4960, 1987, https://doi.org/10.1364/AO.26.004947.

14. N.E. Kouvaris, S. Hata, A. Díaz-Guilera, Pattern formation in multiplex networks, *Sci. Rep.*, **5**:10840, 2015, https://doi.org/10.1038/srep10840.

15. B. Lundstrom, M. Higgs, W. Spain, A.L. Fairhall, Fractional differentiation by neocortical pyramidal neurons, *Nat. Neurosci.*, **11**:1335–1342, 2008, https://doi.org/10.1038/nn.2212.

16. D. Matignon, Stability results for fractional differential equations with applications to control processing, in *Symposium on Control, Optimization and Supervision: CESA'96 IMACS Multi-conference, Computational Engineering in Systems Applications, Lille, France, July 9–12, 1996, Vol. 2*, Gerf EC, Lille, Villeneuve-d'Ascq, 1996, pp. 963–968.

17. C.A. Monje, Y.Q. Chen, B.M. Vinagre, D. Xue, V. Feliu-Batlle, *Fractional-Order Systems and Controls: Fundamentals and Applications, Advances in Industrial Control*, Springer, London, 2010, `https://doi.org/10.1007/978-1-84996-335-0`.

18. J.D. Murray, *Mathematical Biology. I: An Introduction* 3rd ed., Springer, New York, 2002, `https://doi.org/10.1007/b98868`.

19. Q. Ouyang, *Patterns Formation in Reaction-diffusion Systems*, Shanghai Science and Technology Education Press, Shanghai, 2000.

20. B. Tao, M. Xiao, Q. Sun, J. Cao, Hopf bifurcation analysis of a delayed fractional-order genetic regulatory network model, *Neurocomputing*, **275**:677–686, 2018, `https://doi.org/10.1016/j.neucom.2017.09.018`.

21. X. Tian, R. Xu, Hopf bifurcation analysis of a reaction-diffusion neural network with time delay in leakage terms and distributed delays, *Neural Process. Lett.*, **43**:173–193, 2016, `https://doi.org/10.1007/s11063-015-9410-0`.

22. X. Tian, R. Xu, Q. Gan, Hopf bifurcation analysis of a BAM neural network with multiple time delays and diffusion, *Appl. Math. Comput.*, **266**:909–926, 2015, `https://doi.org/10.1016/j.amc.2015.06.009`.

23. A.M. Turing, The chemical basis of morphogenesis, *Philos. Trans. R. Soc. Lond., Ser. B, Biol. Sci.*, **237**:37–72, 1952.

24. C. Vilas, M. García, J. Banga, A. Alonso, Robust feed-back control of travelling waves in a class of reaction–diffusion distributed biological systems, *Physica D*, **237**(18):2353–2364, 2008, `https://doi.org/10.1016/j.physd.2008.02.019`.

25. K. Wang, M.L. Steyn-Ross, D.A. Steyn-Ross, M.T. Wilson, J.W. Sleigh, Y. Shiraishi, Simulations of pattern dynamics for reaction-diffusion systems via SIMULINK, *BMC Syst. Biol.*, **8**:45, 2014, `https://doi.org/10.1186/1752-0509-8-45`.

26. Z. Wu, J. Li, J. Li, S. Liu, L. Zhou, Y. Luo, Pattern formations of an epidemic model with Allee effect and time delay, *Chaos Solitons Fractals*, **104**:599–606, 2017, `https://doi.org/10.1016/j.chaos.2017.09.028`.

27. H. Yin, X. Wen, Pattern formation through temporal fractional derivatives, *Sci. Rep.*, **8**:5070, 2018, `https://doi.org/10.1038/s41598-018-23470-8`.

28. X. Zhang, G. Sun, Z. Jin, Spatial dynamics in a predator–prey model with Beddington–DeAngelis functional response, *Phys. Rev. E*, **85**:021924, 2012, `https://doi.org/10.1103/PhysRevE.85.021924`.

29. H. Zhao, X. Huang, X. Zhang, Turing instability and pattern formation of neural networks with reaction–diffusion terms, *Nonlinear Dyn.*, **76**:115–124, 2014, `https://doi.org/10.1007/s11071-013-1114-2`.

30. H. Zhao, L. Wang, C. Ma, Hopf bifurcation and stability analysis on discrete-time Hopfield neural network with delay, *Nonlinear Anal., Real World Appl.*, **9**(1):103–113, 2008, `https://doi.org/10.1016/j.nonrwa.2006.09.005`.

31. Q. Zheng, J. Shen, Dynamics and pattern formation in a cancer network with diffusion, *Commun. Nonlinear Sci. Numer. Simul.*, **27**(1–3):93–109, 2015, `https://doi.org/10.1016/j.cnsns.2015.02.023`.

32. Q. Zheng, J. Shen, Pattern formation in the FitzHugh–Nagumo model, *Comput. Math. Appl.*, **70**(5):1082–1097, 2015, `https://doi.org/10.1016/j.camwa.2015.06.031`.